Episodic organic carbon fluxes from surface ocean to abyssal depths during long-term monitoring in NE Pacific

Kenneth L. Smith Jr.[a,1], Henry A. Ruhl[a,b], Christine L. Huffard[a], Monique Messié[a,c], and Mati Kahru[d]

[a]Monterey Bay Aquarium Research Institute, Moss Landing, CA 95039; [b]National Oceanography Centre, University of Southampton, SO14 3ZH Southampton, United Kingdom; [c]Aix Marseille Université, Université de Toulon, CNRS, Institut de Recherche pour le Développement (IRD), Mediterranean Institute of Oceanography (MIO), Unité Mixte 110, 13288 Marseille, France; and [d]Scripps Institution of Oceanography, University of California, San Diego, La Jolla, CA 92037

Growing evidence suggests substantial quantities of particulate organic carbon (POC) produced in surface waters reach abyssal depths within days during episodic flux events. A 29-year record of in situ observations was used to examine episodic peaks in POC fluxes and sediment community oxygen consumption (SCOC) at Station M (NE Pacific, 4,000-m depth). From 1989 to 2017, 19% of POC flux at 3,400 m arrived during high-magnitude episodic events ($\geq$mean + 2 σ), and 43% from 2011 to 2017. From 2011 to 2017, when high-resolution SCOC data were available, time lags between changes in satellite-estimated export flux (EF), POC flux, and SCOC on the sea floor varied between six flux events from 0 to 70 days, suggesting variable remineralization rates and/or particle sinking speeds. Half of POC flux pulse events correlated with prior increases in EF and/or subsequent SCOC increases. Peaks in EF overlying Station M frequently translated to changes in POC flux at abyssal depths. A power-law model (Martin curve) was used to estimate abyssal fluxes from EF and midwater temperature variation. While the background POC flux at 3,400-m depth was described well by the model, the episodic events were significantly underestimated by ~80% and total flux by almost 50%. Quantifying episodic pulses of organic carbon into the deep sea is critical in modeling the depth and intensity of POC sequestration and understanding the global carbon cycle.

abyssal community | carbon budget | carbon flux

A major challenge in understanding the oceanic carbon cycle has been estimating that portion of organic carbon escaping the upper water column and being sequestered in the deep ocean (e.g., refs. 1 and 2). Satellite-imaging estimates of surface-ocean color are used to model chlorophyll a (Chla) concentration, net primary production (NPP), and export flux (EF), which are then used to model full water-column attenuation (2–4). These approaches form the basis of deep-sea carbon flux and sequestration estimates in global carbon budgets that contribute to the Intergovernmental Panel on Climate Change Assessment Reports (5, 6). However, they do not account for particulate organic carbon (POC) sinking rates and degradation processes, which can vary according to ephemeral oceanographic features (1, 7–9). Factors affecting sinking velocity of particulate matter such as temperature, viscosity, mineral ballasting, particle size, and composition are likely to vary in association with daily and longer-term oceanographic variations (1, 2, 10–13). Aggregation of POC and ballasting by biogenic and/or lithogenic phases has been linked to episodic flux events (14–16), as has input at higher trophic levels including large zooplankton (17, 18). Thus, we might expect variation in the relationships between surface export and deep-sea carbon processes over time.

There is growing evidence that considerable quantities of POC produced in surface waters can be transported rapidly to abyssal depths, delivering large amounts of fresh (i.e., nonrefractory) material to the sea floor (e.g., refs. 17–19). These high-flux events

can account for significant carbon export from the euphotic zone, and even dominate net carbon export in some regions (20). Such events appear essential to driving key ecosystem processes, including sinking particulate carbon transport and sediment community oxygen consumption (SCOC; e.g., refs. 18, 21, and 22). Evidence from time-lapse cameras and time-series measurements of SCOC at abyssal depths suggest these events also bring important quantities of POC to the deep sea, and potentially balance a long-standing carbon supply and deficit (18, 22). Even though long-term time-series studies have shown that episodic flux events are a typical component of carbon deposition and remineralization on the deep-sea floor (e.g., ref. 21), the frequency, intensity, and duration remain poorly defined. Several critical questions remain: (*i*) Has the intensity and frequency of episodic, high-magnitude flux events changed over time? (*ii*) Is there a temporal relationship between individual surface-ocean EF events and abyssal carbon sequestration processes in the water column and on the sea floor? (*iii*) What portion of overall POC flux reaches abyssal depths during episodic events compared with background conditions?

We examined these questions using a long-term ecological dataset from an abyssal station in the NE Pacific within the

Significance

Ignoring temporal fluctuations in the oceanic carbon budget leads to a significant misrepresentation of the cycling of organic matter from production in surface waters to consumption and sequestration in the abyssal ocean. A 29-year time series (1989 to 2017) of particulate organic carbon (POC) fluxes and sea-floor measurements of sediment community oxygen consumption (SCOC) revealed episodic, high-magnitude events over the past 7 years. Time lags between changes in satellite-estimated export flux, POC flux and SCOC varied from 0 to 70 days. A commonly used model to estimate carbon flux through the water column significantly underestimated the measured carbon fluxes by almost 50%. Episodic pulses of organic carbon into the deep sea must be accounted for to balance the oceanic carbon budget.

California Current Ecosystem (Station M, 34° 50′N, 123° 00′W, 4,000-m depth; 1989 to 2017). Such Eastern Boundary Coastal Upwelling systems can account for over 10% of global new production (23). Station (Sta.) M was chosen in 1989 because of expected high seasonality in surface production manifested in deep-ocean processes (24, 25). Over time it has become evident that interannual and longer-term processes also provide important variation in the area. Ocean basin scale climate forcing has cascading influences on local winds, ocean circulation including upwelling, fronts, filaments, and eddies, and related variations in hydrographic structure, sea surface temperature (SST), and sea surface height (e.g., refs. 26 and 27). El Niño Southern Oscillation forcing has been linked further to changes in nutrient availability, primary production, zooplankton dynamics, POC export flux, and ultimately abyssal sea-floor ecosystem function (e.g., refs. 8, 21, and 28). For example, SST exhibited seasonal and interannual variation from 1989 through 2017 in the region over Sta. M, with increasing peaks during El Niño periods in 1997 to 1998 and 2014 to 2016 significantly exceeding 18 °C (mean + 2 σ; Fig. 1A). Surface Chla concentration, NPP, and EF derived from ocean-color imaging, within a 100-km-radius circle overlying Sta. M, showed significant decreases during these El Niño periods (Fig. 1B). We evaluated lagged relationships between high-magnitude "pulse" events (i.e., ≥1989-to-2017 time-series mean + 2 σ) of surface EF, abyssal POC flux (3,400-m depth; 600 m above bottom), sea-floor detrital aggregate (DA) % cover (4,000-m depth), and SCOC (4,000-m depth). We analyzed

a subset of the time series, from 2011 through 2017, when high-resolution organic carbon supply and demand fluxes were available for both the water column (sediment traps) and at the sea floor (time-lapse camera and mobile sea-floor respirometer) on temporal scales comparable to satellite-derived surface-ocean production (export flux). Lastly, we discuss the implications of our findings in the context of interpreting both observations and model estimates of EF and abyssal carbon fluxes.

Results

Twenty-Nine-Year Time Series: 1989 Through 2017. The POC flux at 3,400-m (600 m above bottom) depth showed seasonality and interannual variability over the entire time series, with the highest peak reaching 57 mg C·m^{-2}·d^{-1} (Fig. 1C). POC flux peaked in spring and summer periods, with highest spikes in 2011, 2016, and 2017. Mean POC flux was 8.1 mg C·m^{-2}·d^{-1} through the entire time series. For years with ≥50% sampling coverage, significant pulses (mean + 2 σ = 22.5 mg C·m^{-2}·d^{-1}) occurred in 2007, 2011 to 2013, and 2016 to 2017, contributing from 25 to 63% of the annual POC flux (Fig. 2).

On the sea floor, detrital aggregate % cover had a time-series mean of 6.4, becoming sharply higher beginning in 2011 compared with the preceding 21-y period (Fig. 1D). Significant peaks (mean + 2 σ = 46.6%) in DA % cover were evident in 2012, 2016, and 2017 exceeding 90%. Short-term seasonal measurements of SCOC were made from 1989 until 2011, with rates generally below the mean of 12 mg C·m^{-2}·d^{-1} for the entire 29-y period (Fig. 1E). Beginning in 2011, the benthic transecting Rover came on-line. This autonomous underwater vehicle provides contiguous measurements of SCOC that revealed elevated rates in 2012 reaching 24 mg C·m^{-2}·d^{-1}, significantly above 18.7 (mean + 2 σ), before declining to lower seasonal peaks in 2016 and 2017.

Seven-Year Time Series: 2011 Through 2017. Mean export flux over this 7-y period was 113.4 mg C·m^{-2}·d^{-1}. Six significant EF peaks exceeded the 1989-to-2017 pulse threshold (139.6 mg C·m^{-2}·d^{-1}), bracketing the low fluxes during the El Niño event in 2015 to 2016 (Fig. 3A). From 2011 to 2017, POC flux mean + 2 σ was 33.1 mg C·m^{-2}·d^{-1}. Six significant POC flux peaks above the 1989-to-2017 mean + 2 σ pulse threshold (22.5 mg C·m^{-2}·d^{-1}) occurred from 2011 to 2017 that could be analyzed from the surface to the sea floor—one each in 2011 and 2012 before decreasing during the El Niño event, and then four more in 2016 and 2017 (Fig. 3B). The mean POC flux over the 7-y period, 11.7 mg C·m^{-2}·d^{-1}, exceeded the entire time-series POC flux mean of 8.1 mg C·m^{-2}·d^{-1}.

Detrital aggregate % cover from 2011 to 2017, mean 14.9%, was more than twice that for the entire time series, mean 6.4% (Fig. 3C). There were five significant DA peaks above the 1989-to-2017 mean + 2 σ threshold (46.6%), two in 2012 following POC pulses in 2011 and three in 2016 and 2017 matching POC peaks over the same period. The longest sustained period of high DA % cover was in summer and fall 2017. Mean SCOC during the 2011-to-2017 period, 12.7 mg C·m^{-2}·d^{-1}, was only slightly higher than for the entire time series (12.1 mg C·m^{-2}·d^{-1}; Fig. 3D). SCOC was significantly higher than the 1989-to-2017 pulse threshold (18.7 mg C·m^{-2}·d^{-1}) during two periods, a major rate increase in 2012 corresponding to a peak in DA % cover and in winter and spring 2015 (Fig. 3C). Lower spikes in SCOC corresponded to the POC flux and DA % cover events in 2016 and 2017.

Pulse Events. Temporal lags and correlations between POC flux pulses at abyssal depths and remineralization on the sea floor were highly variable between each event at Sta. M (Fig. 3). The duration and magnitude of these events, and the time between surface-ocean conditions related to carbon production, delivery
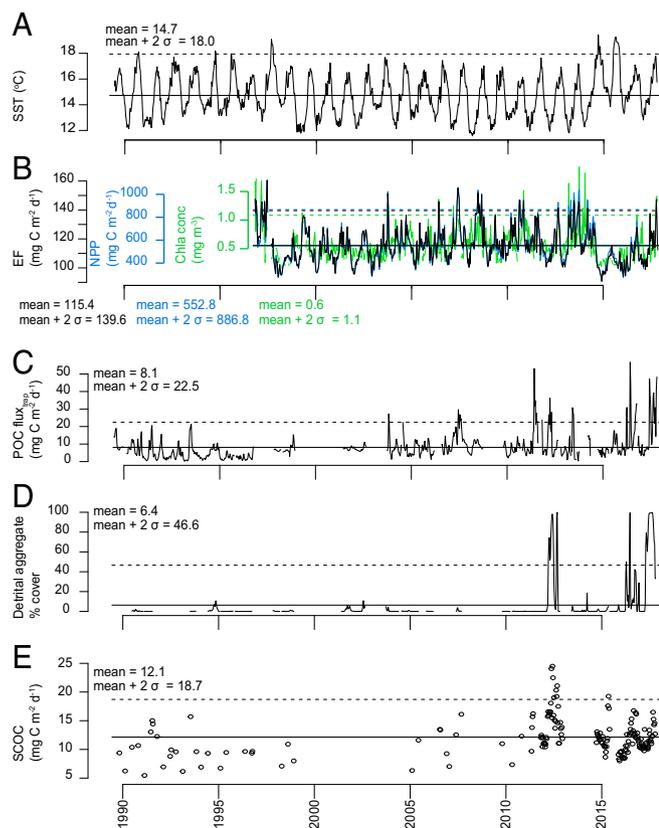
Fig. 1. (A and B) Full Station M time series of sea surface temperature (A) and surface chlorophyll a concentration (green lines), net primary production (blue lines), and export flux (black lines) (B) estimated from satellites with a 100-km radius around Station M. (C–E) Trap-measured particulate organic carbon flux (C), detrital aggregate % cover on the sea floor (D), and sediment community oxygen consumption (E). Time-series mean, and mean + 2 σ threshold, are shown as solid and dashed lines, respectively.
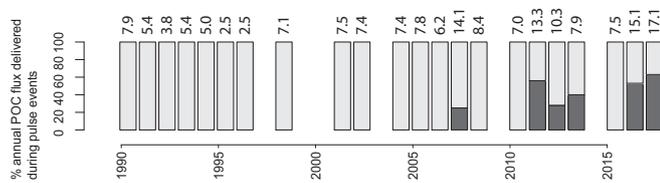
Fig. 2. Contribution of pulse events to annual carbon flux to 3,400-m depth, for years with >50% sampling coverage, based on sediment trap measures. Dark gray bars represent the proportion of annual POC flux that arrived during pulse periods, while light gray bars represent the proportion that arrived during nonpulse periods. Mean annual POC flux (mg C·m^{-2}·d^{-1}) is given above each bar.

of organic carbon to abyssal depths, and remineralization on the sea floor, showed considerable variation. EF and POC flux pulse events were usually, but not always, followed by changes in the carbon flux at greater depths. Three principal components of the carbon cycle from surface production to sea-floor remineralization are EF, POC flux, and SCOC. Six POC flux pulse events exceeding the 1989-to-2017 mean + 2 σ (22.5 mg C·m^{-2}·d^{-1}) were identified and compared across all three of these components: spring 2012, spring, summer, and fall 2016, and summer and fall 2017 (Fig. 3).

The spring 2012 POC flux pulse event (no. 1; 1,480 mg C·m^{-2}) was 23% of the correlated EF (6,340 mg C·m^{-2}) with a 40-d lag (Fig. 3 *A* and *B* and Table 1). The corresponding SCOC (1,220 mg C·m^{-2}) over a 60-d period was 82% of the POC pulse and significantly correlated ($P \leq 0.0005$) with a lag of 70 d. The SCOC event was 19% of the associated EF event. The organic carbon supply at 3,400 m was similar in magnitude to the estimated remineralization on the sea floor exceeding the demand (SCOC) by 18% during this event. It must be noted that our methods did not account for differences in the duration of responses following changes in EF and POC flux. If SCOC response to changes in POC flux is more prolonged than the duration of the POC flux pulse event itself, then we have underestimated the total carbon consumed by the sediment community in response to the POC flux pulse.

The spring 2016 POC flux pulse event (no. 2; 590 mg C·m^{-2}) was preceded by a suggestive increase ($P \leq 0.05$) in EF (2,100 mg C·m^{-2}) 10 d earlier (Fig. 3 *A* and *B*). Twenty days after this POC flux pulse event, there was a significant response ($P \leq 0.0005$) in SCOC (220 mg C·m^{-2}) on the sea floor (Fig. 3*D*). Estimated POC flux during this 20-d event was 28% of the EF and exceeded the remineralization on the sea floor by 2.7 times. In summer of 2016, EF (2,330 mg C·m^{-2}) coincided with the POC flux pulse (no. 3; 1,010 mg C·m^{-2}) with no lag (Fig. 3 *A* and *B*). This 20-d POC flux pulse event was followed 30 d later by a period of increased SCOC (280 mg C·m^{-2}). Supply of POC during this event was 43% of the EF and exceeded the estimated consumption of carbon (SCOC) by 3.6 times (Table 1). The final 2016 POC pulse event in the fall (no. 4; 1,210 mg C·m^{-2}) occurred over a 40-d period from September 26 to November 4. This POC flux event followed a peak in EF (4,940 mg C·m^{-2}) by 10 d (Fig. 3 *A* and *B*), with 25% being collected in the abyssal sediment traps (Table 1). There was a 0-d lag between POC flux and SCOC (540 mg C·m^{-2}), which was not suggestive (Fig. 3 *B* and *D*). The POC supply over this 40-d event was 2.2 times greater than the demand by the sediment community (Table 1).

In 2017, there were two POC flux pulse events, summer and fall. The 30-d summer POC flux (no. 5; 1,180 mg C·m^{-2}) event followed a local peak in EF (3,810 mg C·m^{-2}) by 10 d ($P \leq 0.01$; Fig. 3 *A* and *B*). EF exceeded the POC flux by a factor of three over this period (Table 1). In turn, this POC flux, with a significant lag of 10 d ($P \leq 0.005$), was three times higher than SCOC (370 mg C·m^{-2}). Pulse event no. 6 (2,600 mg C·m^{-2}) was recorded

over a prolonged 80-d period in the fall from September into mid November 2017 (Fig. 3). POC flux followed by 20 d a local peak in EF (10,080 mg C·m^{-2}) and preceded a local peak in SCOC (1,170 mg C·m^{-2}) by 20 d. Over this 80-d period, EF was 3.9 times greater than the POC flux, which in turn was 2.2 times greater than SCOC (Table 1).

A composite illustration showing average estimated fluxes of organic carbon and associated time lags related to the six POC flux pulse events from the surface (EF) through remineralization on the sea floor (SCOC) is shown in Fig. 4*A*. Average EF carbon preceding POC flux pulse events was 4,933 mg C·m^{-2} with a time lag between 0 and 40 d to changes in POC flux (Fig. 4*B* and Table 1). Average POC flux pulse event carbon was 1,345 mg C·m^{-2}. SCOC averaged 633 mg C·m^{-2} with a lag after POC flux of 0 to 70 d. Between January 6, 2011 and December 31, 2017, there were 130 10-d periods for which POC flux, EF, and SCOC data coincided. During this period, summed carbon content was as follows. EF: 117,700 mg C·m^{-2} during nonpulse periods ($n = $ 1,100 d) and 23,600 mg C·m^{-2} during pulse periods ($n = $ 200 d); POC flux: 8,580 mg C·m^{-2} during nonpulse periods ($n = $ 1,100 d) and 6,860 mg C·m^{-2} during pulse periods ($n = $ 100 d); and SCOC: 13,310 mg C·m^{-2} during nonpulse periods ($n = $ 1,100 d)
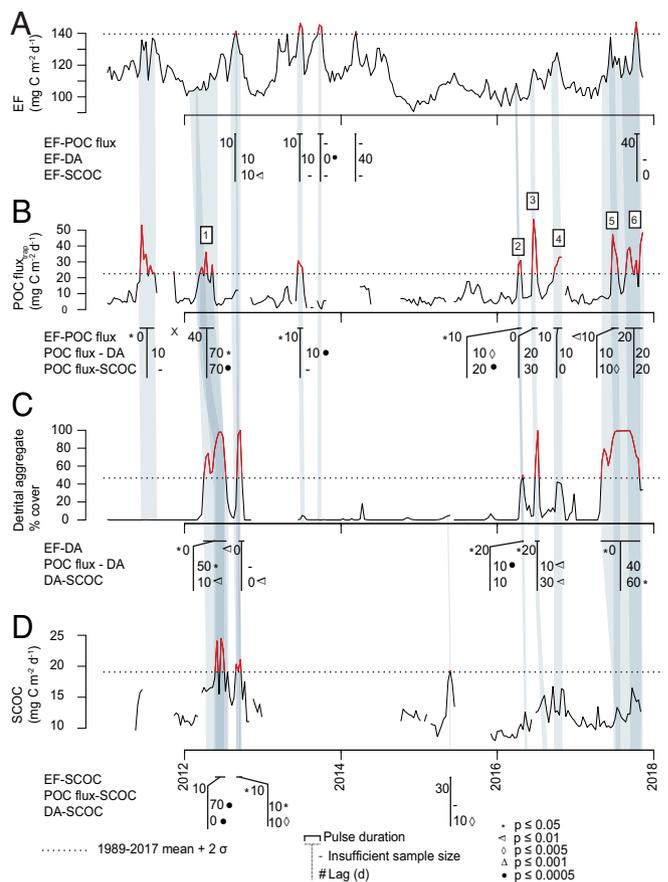
Fig. 3. Time lags in days associated with pulse periods of EF (*A*), POC flux to 3,400 m (*B*), DA % cover (at 4,000 m) (*C*), and SCOC (at 4,000 m) (*D*). Red lines identify periods when values exceeded the 1989-to-2017 time-series mean + 2 σ (dotted lines), the threshold for pulse events used in the analysis. Graphics below the time-series plots show timing of peaks in cross-correlations and lags between the plotted pulse events and EF, POC flux, DA, and SCOC. *P*-value ranges for lagged correlations are noted. The duration of pulses is illustrated as a horizontal line above the associated lags and *P*-value symbols. Transparent gray shading has been added to illustrate the sequence of lags between variables. Numbered POC flux peaks (*B*) refer to events analyzed from surface to sea floor.

Table 1. Carbon content of POC flux pulse events and associated leading EF and lagging SCOC for a window of the same duration as the POC flux pulse event but shifted by the peak lagged correlation determined through cross-correlation analysis

ID	Dates (no. of days)	EF_100 km, mg C·m^{-2}	POC flux, mg C·m^{-2}	SCOC, mg C·m^{-2}
1	3/21/2012 to 5/19/2012 (60)	6,340	1,480	1,220
2	4/9/2016 to 4/28/2016 (20)	2,100	590	220
3	6/18/2016 to 7/7/2016 (20)	2,330	1,010	280
4	9/26/2016 to 11/4/2016 (40)	4,940	1,210	540
5	6/23/2017 to 7/22/2017 (30)	3,810	1,180	370
6	9/1/2017 to 11/19/2017 (80)	10,080	2,600	**1,170**
Average	(42)	4,933	1,345	633
Minimum	(20)	2,100	590	220
Maximum	(80)	10,080	2,600	1,220

The SCOC value in bold was missing one 10-d period. This missing period was infilled from the mean of other 10-d periods in that window.

and 2,660 mg C·m^{-2} during pulse periods ($n = 200$ d) (*SI Appendix*, Table S1). POC flux represented 11% of EF. SCOC represented 103% of POC flux.

Discussion and Conclusions

The observed variation between each POC pulse event provides a challenge when searching for common descriptors to predict future changes in the deep-ocean carbon cycle. While numerous examples of EF events subsequently translated to abyssal POC pulses, this pattern was not consistent. Export flux modeled from satellite data alone was not sufficient for predicting the development and fate of these high-magnitude sinking events that comprise an increasing fraction of annual flux at Sta. M. Temporal and spatial variation in particle export fluxes, subsequent sinking speeds, and remineralization rates with depth determine, in part, how these episodic events develop. Sinking speeds to achieve the observed time lags between EF and POC flux ranged from 85 to 340 m·d^{-1} (not including events when no lag was detected), suggesting the export of particulate matter from surface waters to this abyssal site is not represented well by steady-state assumptions (e.g., ref. 9). The average sinking speed of 234 m·d^{-1} was considerably faster than the 100 m·d^{-1} estimated from cross-correlations of periods through the time series (e.g., refs. 29–31).

Previous work has shown that ecosystem structure and dynamics might explain a significant portion of variation in the biological carbon pump (32, 33). Communities that produce fast-sinking particles (34) are especially important for determining POC flux export from surface waters and transfer to the deep sea. Faster-sinking particles are assumed to experience less exposure to consumption by heterotrophs, and therefore less carbon attenuation, than slower-sinking particles during vertical transport through the water column (35, 36). The high variability we observed in lags between surface and abyssal carbon dynamics related to POC flux pulse events suggests variability in food web dynamics and particle sinking rates. However, we also recognize that correlations with only a few time points describing individual events can contribute to variance in the results. Salp fecal pellets are very fast-sinking (37), carbon-rich particles which can be responsible for significant carbon delivery to the deep sea (36). They were evident during POC flux pulse no. 1 in 2012 (19), for which we estimated a lag of 40 d from EF to POC flux, which elicited a strong SCOC response 70 d after reaching 3,400 m. The fact that some, but not all, POC flux pulse events were followed by depositions of detrital aggregates visible in sea-floor images suggests variability in the biological carbon pump due to clumping of particles in marine snow and larger aggregates (e.g., ref. 38). Variable lags between POC flux pulse events and SCOC

suggest differences in the quality of sinking material, which might trace back to phytoplankton nutrient availability (e.g., ref. 39), ecosystem dynamics and food web processing (e.g., ref. 40), and sinking speeds (e.g., ref. 34).

High-resolution sampling has improved the capability to estimate surface-ocean organic carbon production to sea-floor consumption at Sta. M. Over the period from 2011 to 2017, the remineralization of organic carbon on the sea floor (SCOC) accounted for an estimated 11% of the EF, matching well the measured POC flux (*SI Appendix*, Table S1). Previous analysis using a ratio of monthly and yearly POC flux and SCOC averages from 1989 to 2015 estimated a 37% shortfall in POC flux to account for SCOC over the time series at Sta. M (23).

Global climate models use simplified representations of biological carbon pump processes, including carbon sequestration and deep POC fluxes. The question then arises: How well do model estimates based on upper-ocean variation agree with POC flux time-series data? The "Martin curve" model of remineralization with depth and related models is commonly used to estimate carbon flux with depth (2, 5), with no expectation of estimating episodic fluxes. The attenuation curve typically shows a rapid decline in particulate organic carbon flux with depth in the upper 500 m of the water column, with only a small percentage reaching greater depths (3). This power-law equation is
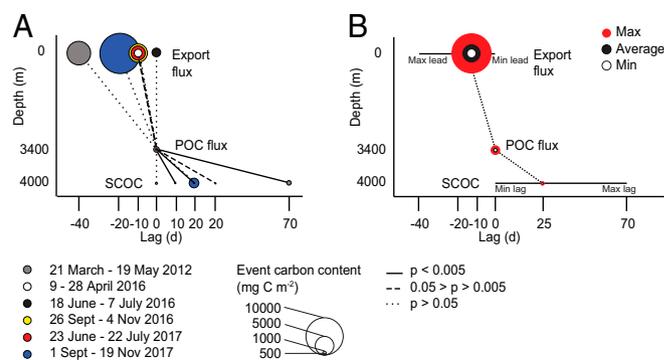
Fig. 4. POC flux pulse event carbon content and lags. (*A*) Carbon content and time lags related to specific POC flux pulse events. (*B*) Average, minimum, and maximum carbon content and time lags from EF to POC flux pulse events to SCOC. For both panels, circle size represents carbon content delivered during the POC flux pulse, along with related EF and SCOC for the same time window shifted by the peak lagged correlation, and line format denotes the *P*-value range of the peak lagged correlation.
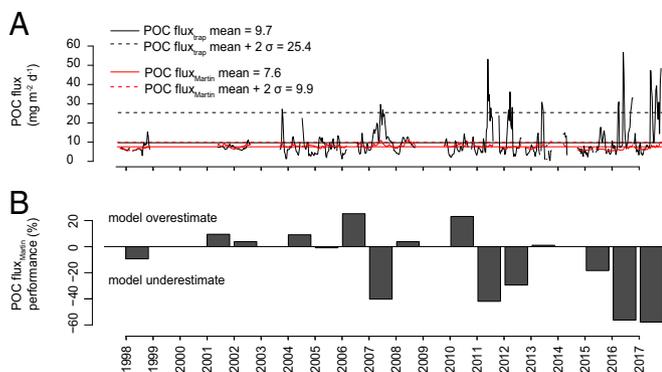
Fig. 5. Performance of Martin POC flux model estimates for Station M from 1989 to 2017 compared with sediment trap measures. (*A*) Full time series. (*B*) Model over/underestimate of POC flux on an annual scale for years with >50% sampling coverage: (POC flux$_{Martin}$ − POC flux$_{trap}$)/POC flux$_{trap}$ 100.

$[f_z = f_{z_0}(z/z_0)^{-b}]$, where z_0 is export depth (here 100-m depth), f_{z_0} is flux at export depth, and f_z is flux at depth z (here 3,400-m depth), and the coefficient of flux attenuation (b) parameter can be set to vary with midwater temperature parameterized with a spatially variable dataset (2). Using this variable b formulation of the Martin curve over time at Sta. M along with satellite-estimated EF, for 10-d periods when trap measurements and EF data were available ($n = 130$), the POC flux at 3,400-m depth (600 m above bottom) is estimated by the Martin curve to be 6.8 ± 0.9 mg C·m^{-2}·d^{-1} when averaged over the period from 2011 to 2017 (*SI Appendix,* Table S1; T at 250-m depth at Sta. M ranged from 6.96 to 8.46 °C). Thus, Martin curve-estimated flux is ~57% of the measured POC flux (average 11.9 ± 10.8 mg C·m^{-2}·d^{-1}). The measured POC flux reaching 3,400-m depth at Sta. M accounted for 11% of the EF during this period, while the Martin curve estimated only 6% of EF (*SI Appendix,* Table S1). This difference between trap measurements and model estimates is evident when examining the 1989-to-2017 POC flux time series as well (Fig. 5). Martin curve estimates of POC flux showed major divergences from trap measurements during high-flux periods, suggesting this model significantly overestimates attenuation during pulse events (Fig. 5*A*; pulse period POC flux trap measured vs. Martin curve POC flux, two-tailed paired Wilcoxon signed-rank test P value << 0.0001, $V = 666$, $n = 36$). However, the Martin curve model was remarkably close in estimating the background POC flux (nonpulse period POC flux trap measured vs. Martin curve model POC flux, two-tailed paired Wilcoxon signed-rank test P value = 0.757, $V = 51{,}678$, $n = 458$). These deviations in the overall POC flux estimates (all periods POC flux trap measured vs. Martin curve model POC flux, two-tailed paired Wilcoxon signed-rank test P value = 0.015, $V = 68{,}832$, $n = 494$) were more evident in recent years (Fig. 5*B*).

Reasons for the measured-versus-model discrepancies could include errors in EF, carbon attenuation rates, and/or model form and application. Biological carbon pump efficiency varies globally (32, 33, 41), and our results suggest temporal changes are also substantial. Export flux here is modeled from satellite estimates of surface Chla, which does not fully reflect changes in available POC for vertical processing and transport (42). Our application of the Martin curve considered variation in attenuation due to temperature (2) but not to other parameters, which can lead to errors when modeling the biological carbon pump, especially in high-export-production situations (32). Our results corroborate the assertion of Marsay et al. (2) that the power-law equation appears to be an oversimplification for the whole water column.

The definition of pulse events influences their accounting. While using multiples of SD to evaluate extreme events is common in climatology research (e.g., refs. 43 and 44), others define extreme events as those exceeding the 95th percentile (e.g., ref. 45). Here the application of a mean + 2 σ threshold equates to the 95th percentile in POC flux and is a reasonably simple and conservative pulse episode definition (*SI Appendix*).

High-magnitude pulse events of POC sinking through the water column can have a major impact on the oceanic carbon cycle and need consideration in future modeling efforts to balance carbon budgets. While models suggest on the order of ≤5% surface production reaching abyssal depths at the global scale (3, 4), at Sta. M we found a much larger percentage reaching the sea floor at 4,000 m (11%) and equally remineralized between 2011 and 2017 (11%; *SI Appendix,* Table S1). These values are even greater during POC flux pulse periods, when an estimated average of 29% of surface production reached abyssal depths (*SI Appendix,* Table S1). These pulses likely play an important role in resolving the long-term carbon deficit reported for abyssal communities including Sta. M (21, 22).

Methods

We defined pulse events according to variation within a 29-y data record (≥1989-to-2017 mean + 2 σ) and then analyzed lagged cross-correlations between ranked EF, POC flux, and SCOC pulse events for a subset of the time series (2011 to 2017) when high-resolution organic carbon supply and demand fluxes were available for the water column (sediment traps) and at the sea floor (time-lapse camera and mobile sea-floor respirometer). Data were binned into commonly aligned 10-d averages. Export flux was generated for a 100-km radius around Sta. M using Kelly et al. (46). Carbon content of pulse events and associated leading/lagging variables were calculated for a window spanning the POC flux pulse, and shifted to correspond to the temporal lag with the peak correlation. POC flux to 3,400 m was modeled using the Martin power-law equation (3) with an attenuation coefficient (b) that varied according to temperature (2). Because debate exists as to whether P values should be interpreted more conservatively when assessing significance of new discoveries (47), we report multiple ranges of P values in the figures. Following the recommendation of Benjamin et al. (47), we used a threshold for statistical significance of $P \leq 0.005$. Correlations with P values $0.005 < P \leq 0.05$ were interpreted as suggestive. Further details about methods can be found in *SI Appendix*.

1. Buesseler KO, Boyd PW (2009) Shedding light on processes that control particle export and flux attenuation in the twilight zone of the open ocean. *Limnol Oceanogr* 54:1210–1232.
2. Marsay CM, et al. (2015) Attenuation of sinking particulate organic carbon flux through the mesopelagic ocean. *Proc Natl Acad Sci USA* 112:1089–1094.
3. Martin JH, Knauer GA, Karl D, Broenkow WW (1987) VERTEX: Carbon cycling in the northeast Pacific. *Deep Sea Res A* 34:267–285.
4. De La Rocha C, Passow U (2007) Factors influencing the sinking of POC and the efficiency of the biological carbon pump. *Deep Sea Res Part II Top Stud Oceanogr* 54:639–658.
5. Yool A, Popova EE, Anderson TR (2013) MEDUSA-2.0: An intermediate complexity biogeochemical model of the marine carbon cycle for climate change and ocean acidification studies. *Geosci Model Dev* 6:1767–1811.
6. Intergovernmental Panel on Climate Change (2013) *Climate Change 2013: The Physical Science Basis. Contribution of Working Group I to the Fifth Assessment Report of the Intergovernmental Panel on Climate Change*, eds Stocker TF, et al. (Cambridge Univ Press, Cambridge, UK).
7. Buesseler KO, et al. (2008) Particle fluxes associated with mesoscale eddies in the Sargasso Sea. *Deep Sea Res Part II* 55:1426–1444.
8. Fisher JL, Peterson WT, Rykaczewski RR (2015) The impact of El Niño events on the pelagic food chain in the northern California current. *Glob Chang Biol* 21:4401–4414.
9. Giering SLC, et al. (2017) Particle flux in the oceans: Challenging the steady state assumption. *Global Biogeochem Cycles* 31:159–171.

ENVIRONMENTAL SCIENCES

10. Alldredge AL, Gotschalk C, Passow U, Riebesell U (1995) Mass aggregation of diatom blooms: Insights from a mesocosm study. *Deep Sea Res Part II* 42:9–27.

11. Passow U, De La Rocha CL (2006) Accumulation of mineral ballast on organic aggregates. *Global Biogeochem Cycles* 20:GB1013.

12. Armstrong RA, Peterson ML, Lee C, Wakeham SG (2009) Settling velocity spectra and the ballast ratio hypothesis. *Deep Sea Res Part II* 56:1470–1478.

13. Iversen MH, Ploug H (2013) Temperature effects on carbon-specific respiration rate and sinking velocity of diatom aggregates—Potential implications for deep ocean export processes. *Biogeosciences* 10:4073–4085.

14. Baldwin RJ, Glatts RC, Smith KL, Jr (1998) Particulate matter fluxes into the benthic boundary layer at a long time-series station in the abyssal NE Pacific: Composition and fluxes. *Deep Sea Res Part II* 45:643–665.

15. Shaw TJ, Smoak JM, Lauerman L (1998) Scavenging of ex^{234}Th, ex^{230}Th, and ex^{210}Pb by particulate matter in the water column of the California Continental Margin. *Deep Sea Res Part II* 45:763–779.

16. Nowald N, Iversen MH, Fischer G, Ratmeyer V, Wefer G (2015) Time series of in-situ particle properties and sediment trap fluxes in the coastal upwelling filament off Cape Blanc, Mauritania. *Prog Oceanogr* 137:1–11.

17. Robison BH, Reisenbichler KR, Sherlock RE (2005) Giant larvacean houses: Rapid carbon transport to the deep sea floor. *Science* 308:1609–1611.

18. Smith KL, Jr, et al. (2014) Large salp bloom export from the upper ocean and benthic community response in the abyssal northeast Pacific: Day to week resolution. *Limnol Oceanogr* 59:245–257.

19. Agusti S, et al. (2015) Ubiquitous healthy diatoms in the deep sea confirm deep carbon injection by the biological pump. *Nat Commun* 6:7608.

20. Stukel MR, et al. (2017) Mesoscale ocean fronts enhance carbon export due to gravitational sinking and subduction. *Proc Natl Acad Sci USA* 114:1252–1257.

21. Smith KL, Jr, Ruhl HA, Kahru M, Huffard CL, Sherman AD (2013) Deep ocean communities impacted by changing climate over 24 y in the abyssal northeast Pacific Ocean. *Proc Natl Acad Sci USA* 110:19838–19841.

22. Smith KL, Jr, Huffard CL, Sherman AD, Ruhl HA (2016) Decadal change in sediment community oxygen consumption in the abyssal northeast Pacific. *Aquat Geochem* 22:401–417.

23. Chavez FP, Toggweiler JR (1995) Physical estimates of global new production: The upwelling contribution. *Upwelling in the Ocean: Modern Processes and Ancient Records*, eds Summerhayes CP, Emeis KC, Angel MV, Smith RL, Zeitzschel B (John Wiley & Sons, New York), pp 313–320.

24. Smith KL, Kaufmann RS, Baldwin RJ (1994) Coupling of near-bottom pelagic and benthic processes at abyssal depths in the eastern North Pacific Ocean. *Limnol Oceanogr* 39:1101–1118.

25. Smith KL, Jr, Druffel ERM (1998) Long time-series monitoring of an abyssal site in the NE Pacific: An introduction. *Deep Sea Res Part II* 45:573–586.

26. Frischknecht M, Münnich M, Gruber N (2015) Remote versus local influence of ENSO on the California current system. *J Geophys Res Oceans* 120:1353–1374.

27. Nagai T, et al. (2015) Dominant role of eddies and filaments in the offshore transport of carbon and nutrients in the California current system. *J Geophys Res Oceans* 120:5318–5341.

28. Di Lorenzo E, Ohman MD (2013) A double-integration hypothesis to explain ocean ecosystem response to climate forcing. *Proc Natl Acad Sci USA* 110:2496–2499.

29. Smith KL, Jr, Kaufmann RS, Baldwin RJ, Carlucci AF (2001) Pelagic-benthic coupling in the abyssal eastern North Pacific: An 8-year time-series study of food supply and demand. *Limnol Oceanogr* 46:543–556.

30. Smith KL, Jr, et al. (2006) Climate effect on food supply to depths greater than 4,000 meters in the northeast Pacific. *Limnol Oceanogr* 51:166–176.

31. Smith KL, Jr, Ruhl HA, Kaufmann RS, Kahru M (2008) Tracing abyssal food supply back to upper-ocean processes over a 17-year time series in the NE Pacific. *Limnol Oceanogr* 53:2655–2667.

32. Francois R, Honjo S, Krishfield R, Manganini S (2002) Factors controlling the flux of organic carbon to the bathypelagic zone of the ocean. *Global Biogeochem Cycles* 16:34-1–34-20.

33. Henson SA, Sanders R, Madsen E (2012) Global patterns in efficiency of particulate organic carbon export and transfer to the deep ocean. *Global Biogeochem Cycles* 26:GB1028.

34. Riley JS, et al. (2012) The relative contribution of fast and slow sinking particles to ocean carbon export. *Global Biogeochem Cycles* 26:GB1026.

35. Giering SL, et al. (2014) Reconciliation of the carbon budget in the ocean's twilight zone. *Nature* 507:480–483.

36. Stone JP, Steinberg DK (2016) Salp contributions to vertical carbon flux in the Sargasso Sea. *Deep Sea Res Part I* 113:90–100.

37. Lebrato M, et al. (2013) Jelly biomass sinking speed reveals a fast carbon export mechanism. *Limnol Oceanogr* 58:1113–1122.

38. Martin P, et al. (2010) Sedimentation of acantharian cysts in the Iceland Basin: Strontium as a ballast for deep ocean particle flux, and implications for acantharian reproductive strategies. *Limnol Oceanogr* 55:604–614.

39. Yool A, Martin AP, Fernández C, Clark DR (2007) The significance of nitrification for oceanic new production. *Nature* 447:999–1002.

40. Wilson SE, Ruhl HA, Smith KL, Jr (2013) Zooplankton fecal pellet flux in the abyssal northeast Pacific: A 15 year time-series study. *Limnol Oceanogr* 58:881–892.

41. Guidi L, et al.; Tara Oceans Coordinators (2016) Plankton networks driving carbon export in the oligotrophic ocean. *Nature* 532:465–470.

42. Behrenfeld MJ, et al. (2016) Revaluating ocean warming impacts on global phytoplankton. *Nat Clim Chang* 6:323–330.

43. Hansen J, Sato M, Ruedy R (2012) Perception of climate change. *Proc Natl Acad Sci USA* 109:E2415–E2423.

44. Huntingford C, Jones PD, Livina VN, Lenton TM, Cox PM (2013) No increase in global temperature variability despite changing regional patterns. *Nature* 500:327–330.

45. Horton DE, et al. (2015) Contribution of changes in atmospheric circulation patterns to extreme temperature trends. *Nature* 522:465–469.

46. Kelly TB, Goericke R, Kahru M, Song H, Stukel MR (2018) Spatial and interannual variability in export efficiency and the biological pump in an eastern boundary current upwelling system with substantial lateral advection. *Deep Sea Res Part I* 140:14–25.

47. Benjamin DJ, et al. (2018) Redefine statistical significance. *Nat Hum Behav* 1:6–10.